CrossMark

ORIGINAL RESEARCH PAPER

The spatial extent of the Deep Western Boundary Current into the Bounty Trough: new evidence from parasound sub-bottom profiling

Michael Horn[1] · Gabriele Uenzelmann-Neben[1]

Abstract Deep currents such as the Pacific Deep Western Boundary Current (DWBC) are strengthened periodically in Milankovitch cycles. We studied periodic fluctuations in seismic reflection pattern and reflection amplitude in order to detect cycles in the sedimentary layers of Bounty Trough and bounty fan, east of New Zealand. There, the occurrence of the obliquity frequency is caused only by the DWBC. Therefore, it provides direct evidence for the spatial extent of the DWBC. We can confirm the extent of the DWBC west of the outer sill, previously only inferred via erosional features at the outer sill. Further, our data allow an estimation of the extent of the DWBC into the Bounty Trough, limiting the DWBC presence to east of 178.15°E. Using the presented method a larger dataset will allow a chronological and areal mapping of sedimentation processes and hence provide information on glacial/interglacial cycles.

Keywords Parasound sub-bottom profiler · Milankovitch cycles · Deep Western Boundary Current (DWBC) · Bounty Trough

✉ Gabriele Uenzelmann-Neben
Gabriele.Uenzelmann-Neben@awi.de

Michael Horn
michael.horn@awi.de

[1] Alfred-Wegener-Institute, Helmholtz-Center for Polar and Marine Research, Am Alten Hafen 26, 27568 Bremerhaven, Germany

Introduction

Thermohaline Circulation is well known to influence global climate and vice versa (e.g. Clark et al. 2002; Kuhlbrodt et al. 2007). One of its components is the Pacific Deep Western Boundary Current (DWBC, Fig. 1a), the largest deep inflow to the Southwest Pacific Ocean (35–40 % volume transport of deep cold water into the Pacific Ocean, e.g. McCave et al. 2008). Further downstream the DWBC passes along the margin of the New Zealand microcontinent (now referred to as Zealandia). Here, it passes along the steep flanks of the Campbell Plateau until reaching the Bounty Trough. The Bounty Trough cuts into the high relief of the Campbell Plateau and Chatham Rise (Fig. 1b). The upper part of the sedimentary cover at the mouth of the Bounty Trough is extensively eroded indicating the presence of the DWBC (Carter and McCave 1997). Extrapolation of seismic units, as defined at ODP Site 1122, into the Bounty Trough has suggested the presence of the DWBC inside the Bounty Trough since about 19.5 Ma. Further, the data show that around 1.7 Ma the core flow position shifted to the south (Horn and Uenzelmann-Neben 2015) contemporaneously with an intensification of the DWBC due to global cooling (Osborn et al. 1983). Thus it is uncertain whether the DWBC has continued to be active further inside the Bounty Trough during the late Pleistocene or whether its influence has been limited to east of the Outer Sill.

The upper 400 m of the sedimentary cover inside the Bounty Trough consists of sediments from two different sources. The first source is the New Zealand's South Island riverine sediments transported onwards as turbidity currents via the Bounty Channel into the Bounty Trough. Sediments of turbiditic origin from the Bounty Channel are only deposited during glacial sea-level lowstands (Carter
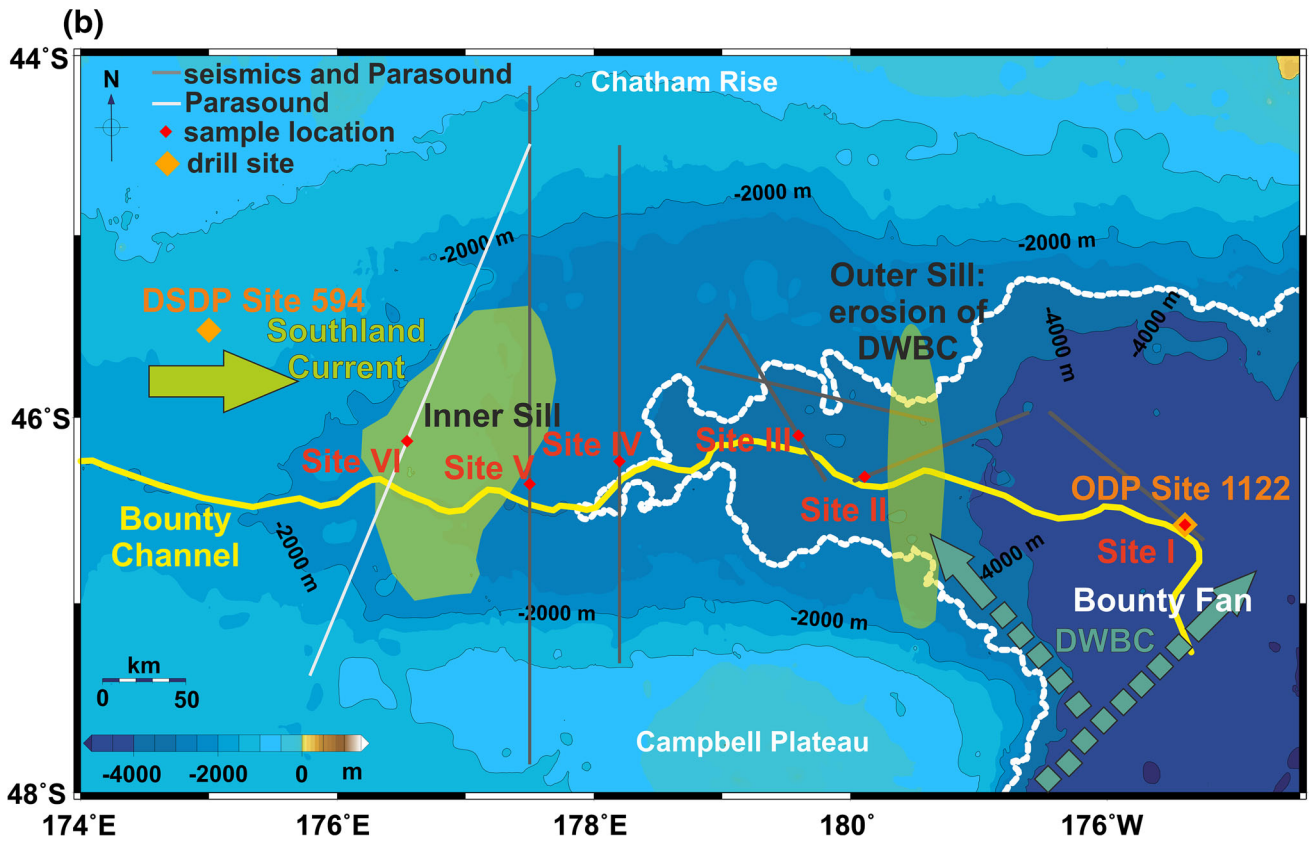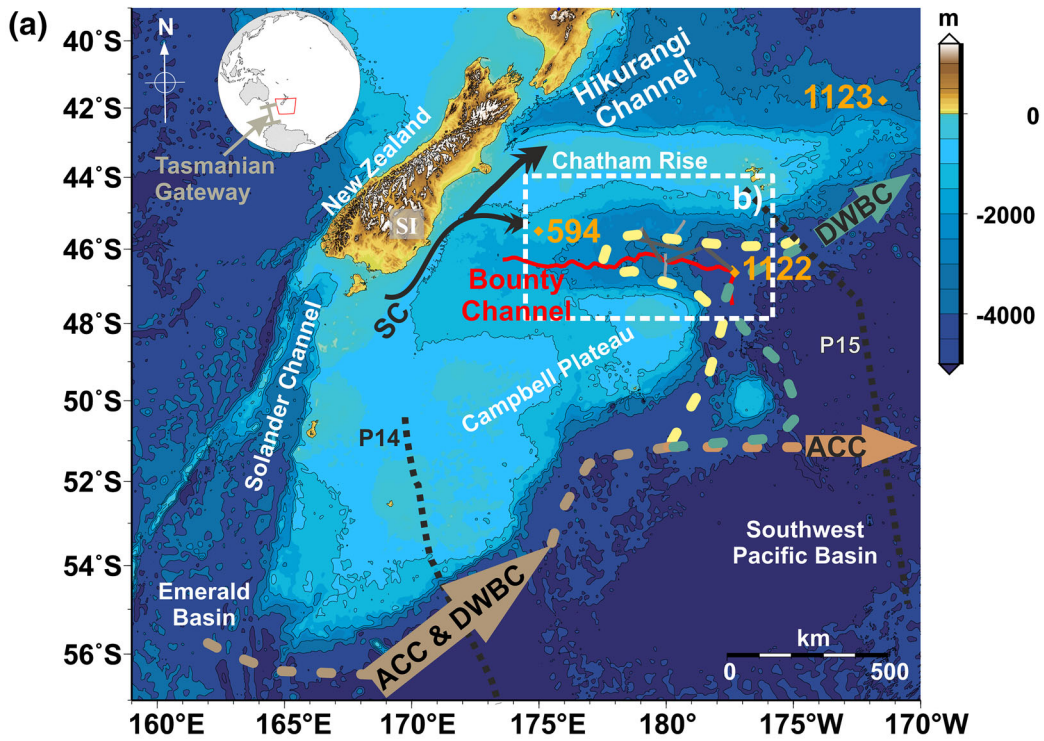
◀**Fig. 1 a** Overview of the Southern Ocean around New Zealand (SI = South Island). *Black lines* indicate the contour lines (every 500 m) of the GEBCO_14 grid (Weatherall et al. 2015), while the *brown dashed arrow* indicates the flow paths of the Antarctic Circumpolar Current (ACC) and the *green* and *yellow arrows* indicate the flow of the Pacific Deep Western Boundary Current (DWBC). Available hydrographic profiles of the World Ocean Circulation Experiment P14 and P15 (Talley 2007) are marked in *dotted black lines*. Deep Sea Drilling Project (DSDP) Site 594 and Ocean Drilling Program (ODP) Sites 1122 and 1123 are marked as orange diamonds. SC = Southland Current. **b** Enlarged map of the Bounty Trough area. ODP Site 1122 and DSDP Site 594 are indicated by *orange diamonds*, sample locations from Site I to Site VI are indicated by *red diamonds*. *Grey Lines* indicate Parasound profiles used for this analysis. *White dotted line* represents the inferred extent of the DWBC from our analysis. The *yellow line* marks the axis of the Bounty Channel

et al. 2004a, b). These lowstands occurred approximately every 100 kyrs during the last 800 kyrs, representing Milankovitch cycles caused by eccentricity (95–125 kyr, e.g. Miller et al. 2005; Zachos et al. 2001). The second sediment source is of hemipelagic origin from the water column (Carter et al. 2004b; Shipboard Scientific Party 2000) either carried or at least influenced by the DWBC. The DWBC itself shows cyclic variations at the obliquity and eccentricity cycles due to periodic reinforcement of the Antarctic Circumpolar Current (expressed at ODP Site 1123; Crundwell et al. 2008; Hall et al. 2001). The occurrence of the obliquity cycle (41 kyr duration) is unique to the sediments deposited under the influence of the DWBC in the Bounty Trough area for the last 800 kyrs. Therefore, the presence of specific Milankovitch cycles, i.e. 41 kyr, can be interpreted as an indication for an active influence of the DWBC on Bounty Channel deposits.

In this study, we use the occurrence of specific Milankovitch frequencies in sub-bottom profiler data to reveal the influence of the DWBC on the sedimentary deposits of the Bounty Channel levee. By converting the two way traveltime (TWT) into age using an age-depth model of a deep-sea borehole we can correlate seismic reflections to age and corresponding Milankovitch frequencies. With these data we can show that the DWBC has been present within the Bounty Trough since 1.7 Ma and we can estimate its spatial variability throughout the last 800 kyrs.

Regional and tectonic setting

The Bounty Trough, east of South Island (New Zealand, Fig. 1a, b), is a failed rift arm formed during the Cretaceous. It is located on thinned continental crust between the Chatham Rise in the north and the Campbell Plateau in the south (Grobys et al. 2007). The Bounty Trough is separated into three different zones by two basement highs showing a

significantly greater slope than the surrounding seafloor (Davy 1993). These steps are termed the Inner Sill and Outer Sill (Carter et al. 1994, Fig. 1b).

Oceanic setting of the Bounty Trough since the Pleistocene

According to Carter et al. (2004a) the general flow path of the DWBC in the Bounty Trough region has been almost unchanged since the early Pliocene (∼5000 ka), but changes in strength have occurred due to climate effects. We thus assume the present oceanic regime also existed during the Plio-/Pleistocene.

The main oceanic influence at the Bounty Trough area close to the Outer Sill results from the DWBC, which enters the area from the south passing along the Campbell Plateau at the base of the Outer Sill (e.g. Carter and McCave 1997; McCave et al. 2008). Before reaching the Bounty Trough area the DWBC is accompanied by the Antarctic Circumpolar Current (ACC) (south of ∼45°S) which has an active influence on flow speed of the DWBC (e.g. Carter et al. 2004b; Crundwell et al. 2008). However, recent research shows that the actual variability of the ACC is minimal (McCave et al. 2014). Thus, only the variability of the DWBC observed by Hall et al. (2001) and Crundwell et al. (2008) is important. Based on the study of sortable silt, $\delta^{13}C$, and subantarctic and subtropical taxa these authors have reported a high periodic variability of the DWBC from sediment sampling directly in the flow path of the DWBC. The variability can be correlated to orbital Milankovitch frequencies. The 41 kyr obliquity cycle in the sediments of ODP Site 1123 has been especially pronounced during the last 1200 kyrs, together with the eccentricity cycles (95 kyr, 125 kyr), as revealed by proxies ($\delta^{18}O$, SST_{ANN-25}) of benthic foraminifers (Crundwell et al. 2008).

The DWBC actively influences sedimentary deposits in its flow path. Examples are a breach in the northern Bounty Channel Levee marking the main core flow of the DWBC (Carter et al. 1990) or the sediment deposition at the Bounty Fan (Carter and Carter 1996). The influence of the DWBC is not limited to the Bounty Fan deposits. The sedimentary cover of the Outer Sill shows erosion of the upper sedimentary unit indicating a vigorous DWBC in recent times. From this area of erosion, a limb of the DWBC is proposed to enter the Bounty Trough (Carter and McCave 1997), but its extent is not known. This in turn can influence the shallower flows above the DWBC and may thus affect New Zealand's climate conditions by influencing the temperature and eastward extent of the surface waters and impacting wind strength (e.g., Crundwell et al. 2008; Hall et al. 2001).

Above the DWBC the Southland Current (Fig. 1b) flows from west to east through the Bounty Trough (Lu et al. 2003; Neil et al. 2004). A periodic strengthening is also visible for the Southland Current. At least during the Last Glacial Maximum the Southland Current showed enhanced flow speeds and during the last interglacial the flow speeds were lower (Neil et al. 2004). Thus we assume that this behaviour was true also for the last 800 kyrs.

Sediment supply into the Bounty Trough since the Pleistocene

The Bounty Trough contains a transport conduit for terrigenous sediments, the Bounty Channel (Carter et al. 2004a, b). Sediment transport in the channel and related deposition started already during the Pliocene (~3.5 Ma) and was fully established by ~2.2 Ma (Shipboard Scientific Party 2000). Sediments were derived from erosion of the Southern Alps on the South Island of New Zealand. Rivers transported the sediments to the shelf edge, where they were injected into offshore currents (Carter et al. 2004b; Shipboard Scientific Party 2000). During sea-level highstands turbidity currents bypassed the head of the Bounty Trough, and via the Southland Current were transported into the Hikurangi Channel further north (see Fig. 1a, Carter and Carter 1993; Carter et al. 2004b). During sea-level lowstands associated with glacial periods, terrigenous sediments reached the deep sea and were deposited as turbidites inside the Bounty Trough and on the Bounty Fan (Carter et al. 1994, 2004b; Shipboard Scientific Party 2000). This has been confirmed by piston cores (Carter and Carter 1988). Deposits can be observed as two levees, the northern levee (in flow direction on the left) being higher than the southern levee due to Coriolis force (Carter and Carter 1996). Since the Mid Pleistocene Transition (~800 ka) the sea-level lowstands occurred roughly with a 100 kyr cyclicity (e.g., Crundwell et al. 2008; Naish et al. 2009; Zachos et al. 2001). We thus would expect pulses of sediment input, which show a cyclicity of roughly 100 kyrs. Further sediment sources for the Bounty Trough area are hemipelagic sediments from the water column. The DWBC itself also transports sediments but no bottom current deposits during the Pleistocene have been reported (Carter et al. 2004b). The upper sedimentary column is primarily dominated by terrigenous sediments interbedded with hemipelagic sediments (e.g. Carter et al. 1994, 1999).

Materials and methods

Available data and data processing

Our study is based on sub-bottom profiles acquired during RV Sonne cruises 169 (Gohl 2003) and 213/2 (Tiedemann et al. 2012) with an Atlas Parasound III P70 system. The Atlas Parasound transducer transmits two different frequencies between 18 and 33 kHz with a short duration (Pulse type: continuous, pulse length between 2 and 16 ms) and a parametric frequency of the difference of these two frequencies due to nonlinear interaction of finite amplitudes in the water (Atlas Hydrographic GmbH 2010; Tiedemann et al. 2012). For more details about operation modes please refer to chapter 8 of Schiel (2009) and for pulse shape to Spiess (1992). During both cruises this parametric frequency was adjusted to 4 kHz.

This paper uses the 4 kHz parametric frequency data, part of such a profile is shown in Fig. 2. The 4 kHz signal penetrates deeper into the sedimentary column (up to 200 m, Atlas Hydrographic GmbH 2010) than the other two frequencies. On-board processing included subtraction of the average amplitude to remove the DC Offset (bias). Further, the envelope function of the full waveform of the signal was calculated to increase the coherency of the signal and to reduce disk space needed. We have applied an additional bandpass filter between 2 and 6 kHz to eliminate noise generated by the ship and other instruments (Spiess 1992). We did not apply any gain to the data. Applying a time dependent gain would also increase noise in the lower part of the recording and was omitted. Evaluation of the occurrence of the DWBC is based on six profiles crossing the Bounty Channel northern levee (Fig. 1b).

Method to reveal Milankovitch cycles in sub-bottom profiler data

We adapt the method of Weigelt and Uenzelmann-Neben (2007) to analyse the occurrence of Milankovitch cycles in our sub-bottom profiler data. According to Hall et al. (2003) a strong periodic forcing is observed in sortable silt of ODP Site 1123 for the Middle Miocene. Here this variation is also linked to periodic strengthening of the DWBC due to orbital forcing. This means that this periodic forcing has a direct effect on the deposited material. For ODP Site 1122 no direct grain size measurements have been carried out. However, the sedimentary composition (silty clay interbedded with fine sand turbidites, very fine sand turbidites, silty clay and/or fine sand and silt, or fine sand silt; Shipboard Scientific Party 2000) implies that the grain size also varies in the upper sedimentary column. Turbidites vary between fine sand and sand in grain size. Between these turbidites silty clay is found (Shipboard Scientific Party 2000). The sedimentary composition of the Bounty Fan is attributed to four different aspects: magnitude of glacial lowstand (last 800 kyrs every 100 kyrs), seismicity (not regular), sediment supply (as turbiditic pulses during sea-level lowstands, i.e. glacial periods which show a cyclicity of roughly 100 kyrs, see "Sediment
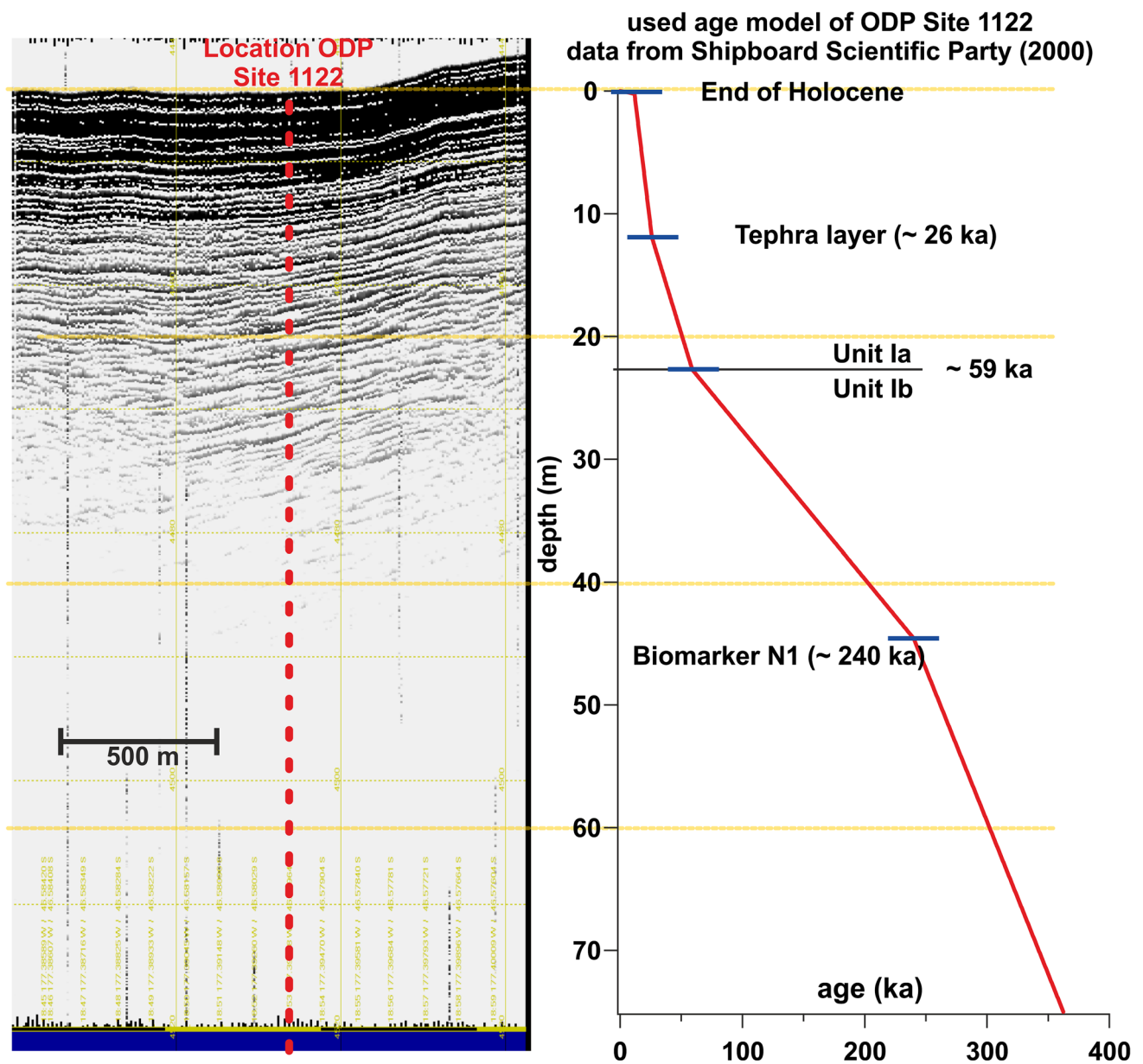
Fig. 2 Data example as depth versus age graph of Parasound Profile at Site I, the location of ODP Site 1122, with the corresponding age derived from the core samples in *blue* [taken from Shipboard Scientific Party (2000)]

supply into the Bounty Trough since the Pleistocene" section), and influence of the DWBC (every 41 kyr Crundwell et al. 2008; Shipboard Scientific Party 2000). As variations in grain size exist and an influence on the composition of the sedimentary fan deposits is attributed to the DWBC (inflow of cold LCDW has had an effect on the deposition of carbonate, diagenesis, increased flow strength on bypass of sediment), we can transfer the results from ODP Site 1123 to the Bounty Trough region and assume that the observed periodic signal of 41 kyr length is no artefact but can be attributed to the DWBC.

Therefore, the following procedure has been performed: In a first step the amplitudes (instantaneous amplitude) have been digitized from the Parasound sub-bottom data for Fourier Transformation to reveal periodic signals. As in Weigelt and Uenzelmann-Neben (2007), we have not applied any filter or windowing to the Fourier Transformation. Analysis of periodic signals is limited to 800 kyrs in age, to meet the assumption made in "Sediment supply into the Bounty Trough since the Pleistocene" section that the DWBC varies with a 41 kyr cycle and that this can be seen in a cyclicity of the impedance of the sediments. In a second step, the TWT of periodic amplitude signals is converted to depth using P-wave velocity functions, then to age using models from boreholes, followed by a conversion to age frequencies for comparison to Milankovitch

cyclicity (Fig. 3; Weigelt and Uenzelmann-Neben 2007). From these data, age frequencies are easily calculated by inversion. The conversion of TWT into age depends on the location of each site and is explained below. Calculations have been carried out using the spreadsheet application IGOR Pro 5. Frequency analysis (Fast Fourier Transform) has been carried out using the method first developed by Cooley and Tukey (1965).

We have chosen six different sites (Site I to Site VI) along the Bounty Channel axis to evaluate the spatial occurrence of different Milankovitch cycles. Each site location is chosen at the crest of the northern levee where a high sedimentation rate prevailed during the Pleistocene (Fig. 1b).

Site I (Fig. 2) was chosen at the location of ODP Site 1122 to have a direct correlation to the age and velocity models for Site 1122. Conversion of TWT into depth was done using the P-wave velocity calculated from density sampling for the upper sedimentary column (density data published by Shipboard Scientific Party 2000, calculations following Erickson and Jarrard 1998). The subsequent conversion from depth to age was adapted from the age-depth model of ODP Site 1122, derived by Horn and Uenzelmann-Neben (2015) from biomarkers, lithologic boundaries and a tephra layer.

In addition to this location five other locations (Fig. 1b) were chosen to evaluate whether the spectrum shows prominent peaks at Milankovitch frequencies. For Sites II and III the same age-depth model and velocity profile were used as for Site I. Sites IV to VI are too far away from ODP

Site 1122 to be treated in the same manner. For depth conversion a constant interval velocity of 1550 m/s (P-wave velocity for the upper 100 m of the sedimentary column, Horn and Uenzelmann-Neben 2015) was used. Sedimentation rates were set to 20 cm/kyr for location IV, 12.5 cm/kyr for locations V and 8.5 cm/kyr for Site VI. Sedimentation rates for sites IV and V are based on a prominent reflection LP (top late Pleistocene) identified in seismic reflection data interpreted by Uenzelmann-Neben et al. (2009). Site VI was not crossed by seismic reflection data. The sedimentation rate for this location was taken from an old core in the upper Bounty Trough where the highest sedimentation rate was measured to be 8.5 cm/kyr in the upper 3 m (Griggs et al. 1983). We are aware that sedimentation rates change during different Milankovitch cycles. But since there are no deep drilling sites close to Sites IV to VI we have to assume a linear sedimentation rate.

The method of Weigelt and Uenzelmann-Neben (2007) has been developed for seismic reflection data. To use it for sub-bottom profiler data, we have to account for the differences in resolution and depth of penetration. One critical point is the resolution of Milankovitch cycles with seismic methods. The used setup is capable of penetrating up to 200 m of unconsolidated sediment (Atlas Hydrographic GmbH 2010). Typical penetration depths of 50–130 m are achieved. Sedimentation rates for the area of interest are between 8.5 and ~38 cm/kyr (approximated sedimentation rate for the upper sedimentary column of ODP Site 1122 (Shipboard Scientific Party 2000); used for error estimation of the method). Depending on location and sedimentation rates, ages of penetrated sedimentary sequences thus range from 120 to 1500 kyr. The frequency (4 kHz) allows a theoretical vertical resolution of approximately 10 cm at the seafloor, thus theoretically resolving 0.263 kyrs. Uncertainties arise from conversion of the TWT to depth and later to age. While the uncertainty by conversion from TWT to depth can be neglected (<3 % based on a velocity variation of 50 m/s and a TWT uncertainty of 0.001 ms), the error of the sedimentation rate plays an important role. For Sites I to III we used the age model derived by Horn and Uenzelmann-Neben (2015). The linear trend in the upper sedimentary column (Fig. 2) and the lack of published age uncertainties for the biomarkers and tephra layers make it difficult to estimate an age error. Therefore, we assume a large uncertainty range of 20 %. For Sites IV to V, the sedimentation rate is calculated from depth migrated seismic reflection data (Uenzelmann-Neben et al. 2009). TWT difference between seafloor and the lower Pleistocene reflections have been picked from seismic data. This can be done with high accuracy (up to 1 m) but we will also assume an uncertainty range of 20 % as we use only one horizon for this
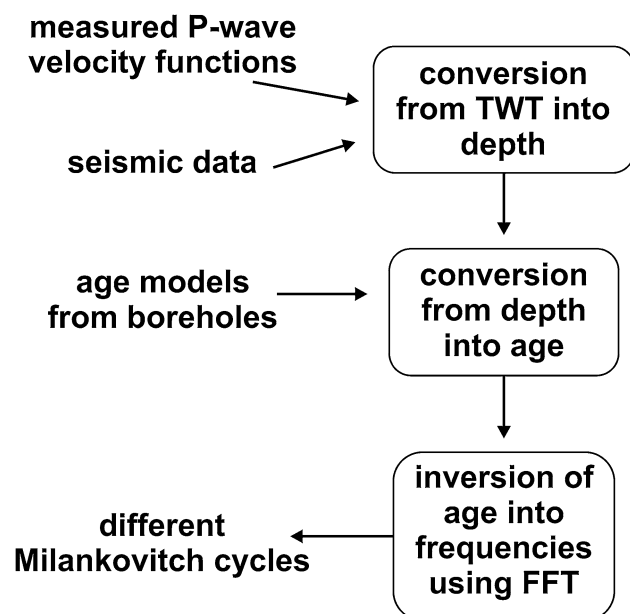
Fig. 3 Flowchart showing the workflow of inverting the seismic data into the different Milankovitch cycles

estimation, data was depth-converted using picked velocities and we can only assume a constant sedimentation rate due to the lack of intermediate dated horizons. The sedimentation rate for Site VI is taken from Griggs et al. (1983). We will assume an error of 20 % as no age error is given and the sedimentation rate is assumed to have been constant for the whole Pleistocene. Thus this uncertainty is transferred to the age of different reflections and the theoretical age resolution of 0.263 kyrs cannot be achieved. The highest resolution achievable is thus assumed to be 8.2 kyrs (for the obliquity cycle) to 20 kyrs (eccentricity cycles around 100 kyrs). These error ranges are still small enough to derive two separate peaks around both frequencies.

Observations

We infer an active influence of the DWBC on deposition at Site I (approx. 4400 m water depth) based on hydrographical findings (Reid 1997; Warren 1973), sediment cores (Carter and Carter 1996) and profiler data (Carter and McCave 1997). Here (Fig. 4, green curve), a peak near the frequency of 24×10^{-3} kyr^{-1} (41 kyr obliquity cycle) can be identified. Its width corresponds to the uncertainties of the age-depth model (8.2 kyrs grey area, Fig. 4) used for the conversion. A spectral peak at a frequency of 8×10^{-3} kyr^{-1} [125 kyrs cycle length (cl)] and another one at 12.5×10^{-3} kyrs^{-1} (80 kyrs cl) can also be observed.

The other investigated sites have been chosen west of the Outer Sill. Site II (approx. 3400 m water depth, yellow in Fig. 4) and Site III (approx. 3200 m water depth, red in Fig. 4) are located close to the Outer Sill. Both Site II and Site III show a frequency peak near 24×10^{-3} kyr^{-1} ($\sim$41 kyr cl) well inside the error margin of 8.2 kyrs (grey area in Fig. 4). Site II shows no pronounced peak at a frequency of 10×10^{-3} kyr^{-1} (100 kyrs) while frequencies lower than 15×10^{-3} kyr^{-1} (67 kyr cl) are almost completely absent at Site III. Site IV (blue in Fig. 4) is located at approximately 2800 m depth. Here, different frequencies appear. A first frequency peak is observed around 13×10^{-3} kyr^{-1} ($\sim$76 kyrs cl) and a second around 10×10^{-3} kyr^{-1} ($\sim$100 kyr cl). Higher frequencies, especially the obliquity frequency of 24×10^{-3} kyr^{-1} ($\sim$41 kyr cl) are not observed. Site V at 2700 m water depth (black in Fig. 4) shows the first peak at 18×10^{-3} kyr^{-1} (56 kyr cl), outside the 41 kyr uncertainty and a pronounced peak around 11×10^{-3} kyr^{-1} (90 kyr cl). Site VI at approximately 2500 m water depths is the most western site of our analysis. Here, the main frequency peak is around 10×10^{-3} kyr^{-1} (100 kyr cl) and the peak around 13×10^{-3} kyr^{-1} (76 kyr cl) observed at Sites IV and V is almost absent. Sites IV to VI exhibit a

second peak between 5 and 6×10^{-3} kyr^{-1} (166–200 kyr cl). These peaks represent cycle lengths of approximately double the length of 100 kyrs cycles.

Discussion

Resolution of cycles

Our main goal is to use Parasound sub-bottom profiler data to resolve the presence of the 41 kyr obliquity cycle. Thus, we have to make sure our data can resolve these cycles. Three important parameters are crucial for a cycle to be resolved, (1) minimum vertical resolution, (2) the sampled interval of sub bottom profiler data, and (3) the accuracy of the age-depth model.

1. Vertical resolution is limited by the used frequency of the Parasound system. To be able to resolve two different reflectors creating a reflection they have to be spaced at least one quarter of the wavelength ($\sim$10 cm at the seafloor) to be recognized as individual events (Sheriff and Geldart 1982). With sedimentation rates between 8.5 and 38 cm/kyr, 41 kyrs are represented by sedimentary deposits of at least $\sim$3.5 m, thus being resolvable as individual events.

2. The analysed interval has to be long enough to incorporate at least two full cycles of the cyclicity we want to observe. Longer periods cannot be analysed reliably because of aliasing. For the specific example of the 41 kyr obliquity cycle we need an age range of >82 kyrs penetrated by sub bottom profiler data. This is fulfilled at all six sites as the minimum age range imaged is $\sim$100 kyrs at Site I. All other sites exhibit at least 135 kyrs of age range and can contain four full cycles or more.

3. The uncertainties in the age-depth models used for age conversion are also a source of discrepancies. In our case uncertainties are estimated to be 20 % of the age value. This uncertainty range is small enough to distinguish the 41 kyr Milankovitch cycle ($\pm$8.2 kyrs) from other cycles such as 100 kyrs ($\pm$20 kyrs). However, peaks will not be as pronounced but exhibit a broader appearance. The corresponding uncertainty ranges are marked in grey in the corresponding frequency analyses (Fig. 4).

For the 100 kyr cyclicity of the Bounty Channel only the second point needs further consideration as longer time periods have to be sampled to observe such cyclicity. For Site I to III the sampled interval is not long enough, as it does not reach an age interval of 200 kyrs. Thus spectral analysis of Sites I to III cannot unequivocally identify these frequencies. If 100 kyrs cycles are present at Sites I to III
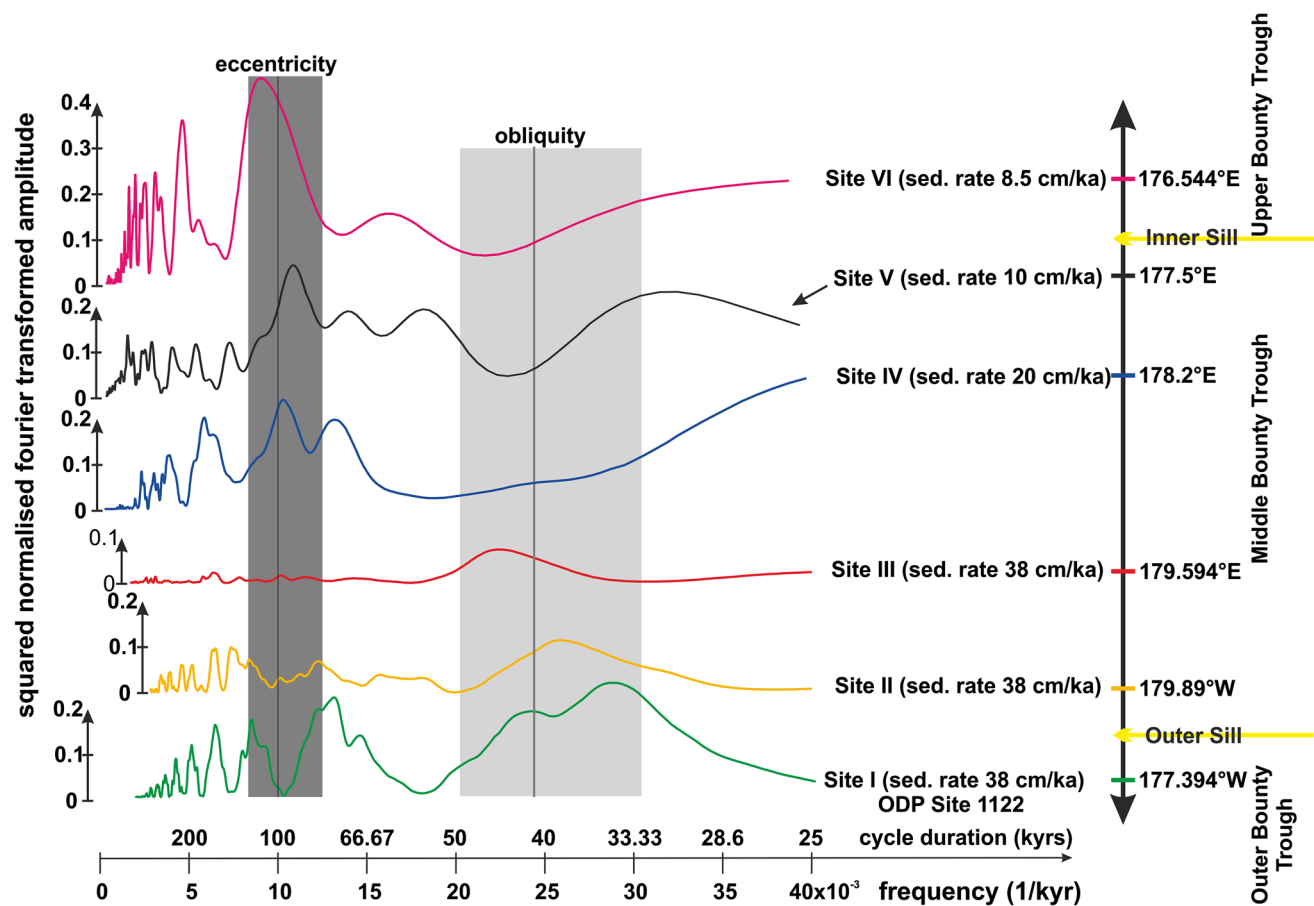
Fig. 4 Spectral analysis of Parasound data from Site I (*lowermost*) to Site VI (*uppermost*). The *grey* areas indicate the uncertainty ranges for the obliquity cycle (41 kyr cycle) and the eccentricity cycle (125–95 kyr cycle) of the frequency bands

they remain unresolved in the type of data used in this study. For Sites IV to VI depth penetration reaches values between 800 and 1200 kyrs. Here, the Bounty Channel cyclicity can be resolved.

Validation of the method at Site I (ODP Site 1122)

ODP Site 1122 lies directly under the influence of the DWBC, which is confirmed by borehole (Shipboard Scientific Party 2000), hydrographical (Warren 1973) and seismic data (Carter and McCave 1997; Horn and Uenzelmann-Neben 2015). Therefore, if our method is valid, the spectral analysis should show a peak for the 41 kyr frequency cycle (24×10^{-3} kyr^{-1}). The corresponding curve of the frequency analysis (Fig. 4, green curve) shows this peak. Thus the spectral analysis is capable of revealing the presence of the DWBC influence on sediment deposition. The frequency peak around 24×10^{-3} kyr^{-1} ($\sim$41 kyr cl) is split into two peaks. This can be explained with the resolution and linearity of the age-depth model of ODP Site 1122. Both peaks are in a range of the ± 8.2 kyrs of the 41 kyr cycle. To validate these results we have also

performed spectral analysis of the physical properties data from ODP Site 1122 to show that these data also reveal a cyclic signal. We have used the age model of Horn and Uenzelmann-Neben (2015) for conversion of depth to age and then calculated frequency and Fourier Transformation. Our first choice parameter would be the seismic impedance of the sediment. Unfortunately, the P-wave velocity logs are not available for Site 1122 as velocity measurements failed in the upper 300 meters of the core (Shipboard Scientific Party 2000). However, many analyses of relation between P-wave velocity and density of clastic sediments have shown that P-wave velocity can directly be derived from density via empiric relations (e.g. Erickson and Jarrard 1998; Hamilton 1978; Nafe and Drake 1957). This implies that the velocity shows exactly the same trend as the density and that the density is an adequate proxy for the impedance. Thus, we only perform this analysis on the density log from multi sensor track of ODP Site 1122. Additionally, we have calculated the first derivative of the density as reflections are normally created by impedance contrasts. Figure 5 shows a comparison of sub-bottom profiler amplitude (Fig. 5a), density data (Fig. 5b) and the

first derivative of density (Fig. 5b) versus the calculated ages of Horn and Uenzelmann-Neben (2015).

Figure 5 shows that the amplitude of the sub-bottom profiler data is linked to the density variations. Additionally, Fig. 5 shows that a 41 kyr periodicity can also be assumed for the density and derivative of the density as multiple peaks occur in such periodicity (marked violet in Fig. 5). As the first derivative of density is proportional to the impedance contrast we have performed Fourier

Transformation of the dataset shown in Fig. 5b. The spectrogram of the first derivative of the density (Fig. 6) clearly shows the occurrence of a cycle of 41 kyr (24×10^{-3} kyr^{-1}) and also a peak linkable to the 100 kyr cycle (10×10^{-3} kyr^{-1}).

We have shown that two different methods sufficiently independent from each other give the same result concerning the dominant frequencies. Together with the information presented in "Sediment supply into the Bounty
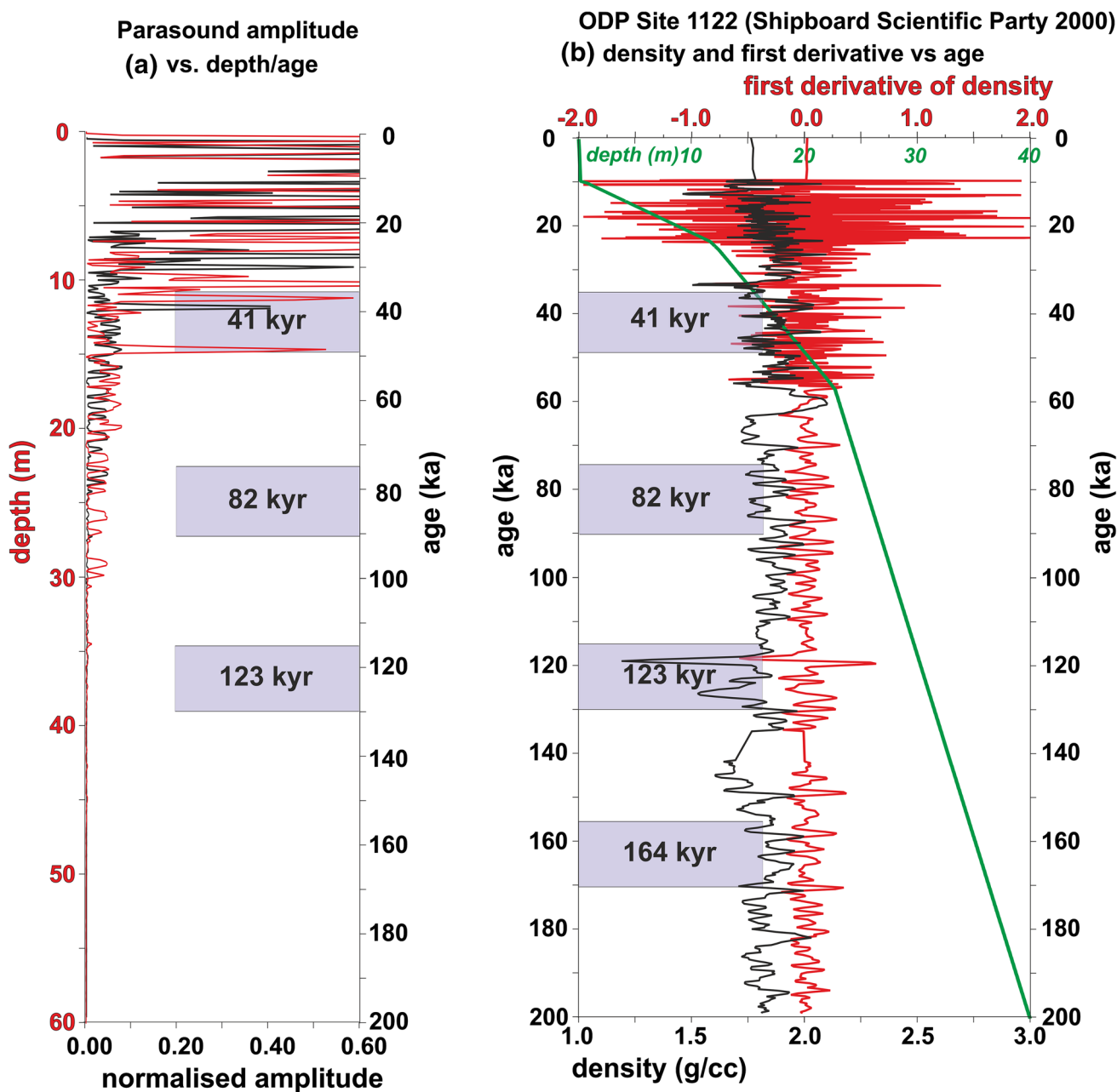
Fig. 5 a Data example of Parasound signal from Site I showing age (*black*) versus depth (*red*) graph The *violet* areas mark the time span with error range where we expect reflections to occur. The location of this trace is almost equal to ODP Site 1122, see Fig. 1b and 3;

b Density measurement (*black*) and first derivative of measured density (*red*) of ODP Site 1122 in the upper 40 meters (*green line*, scale on top) plotted versus age. *Violet* areas again mark the expected range of a periodic signal

Trough since the Pleistocene" section, the only known process able to create the 41 kyr cycle at Site I is variation of the DWBC. This result has two consequences. (1) Like Weigelt and Uenzelmann-Neben (2007) we are able to reveal climate forcing by changes in sediment compositions expressed as impedance contrasts (i.e., as the result of grain size variability and/or changes in composition resulting in strong density contrasts), and (2) the 41 kyr cycle (24×10^{-3} kyr^{-1}) occurrence can be related to the influence of the DWBC. Additionally, our analysis does not rely on specific sediment components such as benthic foraminifers to reveal a periodic forcing as done by Crundwell et al. (2008), and the areal extent of processes caused by Milankovitch cycles can be assigned to definite areas just by surveying an area, provided information concerning sedimentation rates is available and penetration depth is large enough to resolve at least two cycles. This in turn can lead to further inferences, as described in the next section.

Spatial extent of the DWBC into the Bounty Trough

Frequency analyses at Sites II and III clearly show the 24×10^{-3} kyr^{-1} frequency (41 kyr cl) peak (Fig. 4, yellow and red curves). It is shifted a bit to the lower frequencies at Site III and slightly to higher frequencies at Site II, but within the expected uncertainty. This observation confirms the influence of the DWBC inside the Bounty Trough west of the Outer Sill. Due to low penetration and resulting age range it is not possible to examine the presence of cycles of 100 kyr length.

Sites IV to VI have a higher penetration of at least 150 ms TWT ($\sim$120 m) and a lower sedimentation rate, which extends the age range to 800 kyrs. Therefore, we expect the 100 kyrs cycle to be more pronounced and the 41 kyr cycles should be clearly visible if present. Figure 4 shows that Sites IV to VI (Fig. 4, curves in blue, black and magenta) all show a spectral peak around the 100 kyr cycle implying the influence of the Bounty Channel deposits. A
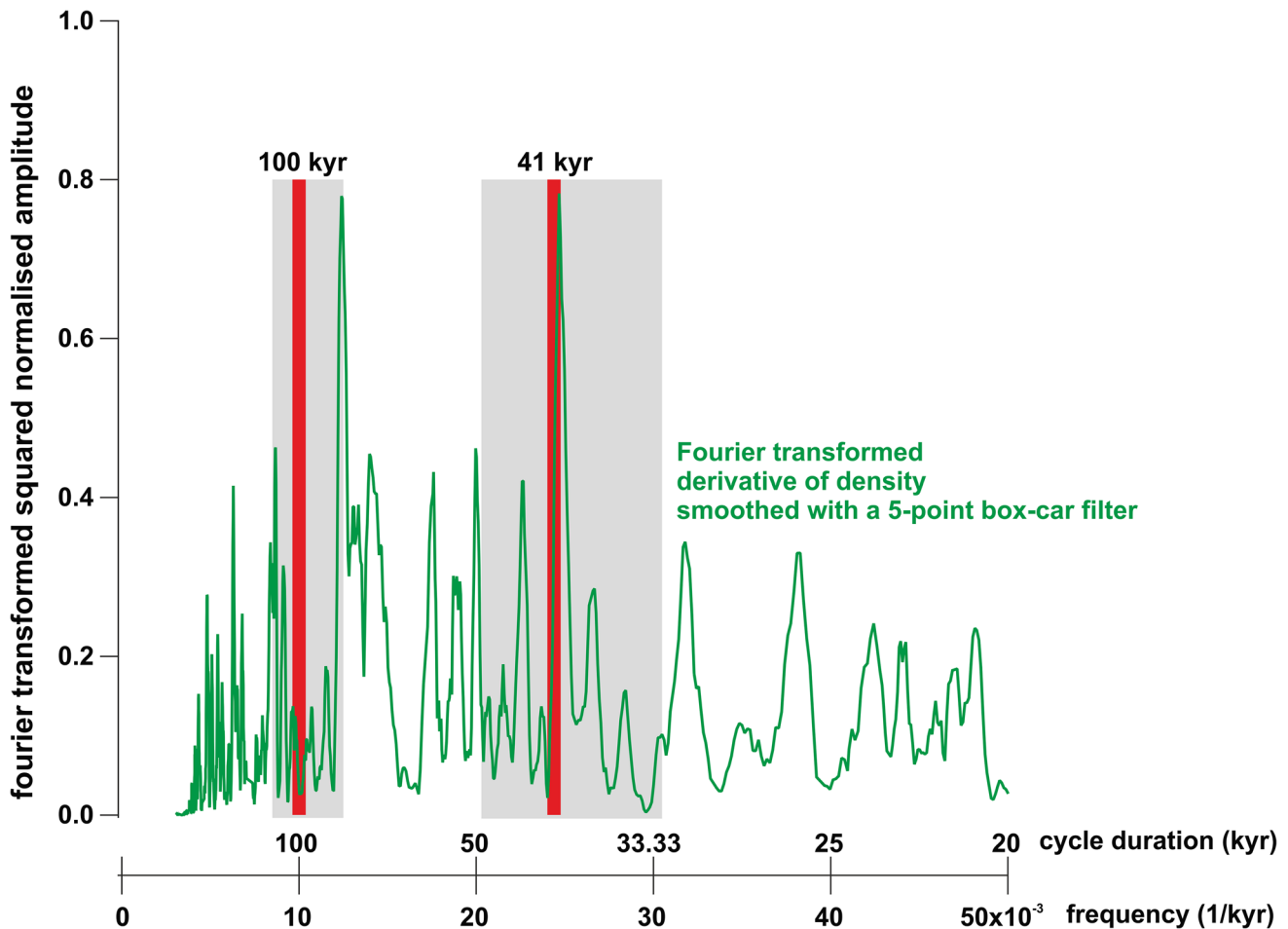
Fig. 6 Fourier transformed signal of the first derivative of the density smoothed with a box filter with 5-point box-car filter. The *grey* marked areas around the marked frequencies indicate the uncertainties of each frequency. Note the pronounced peak around 24×10^{-3} kyr^{-1} (corresponding to 41 kyr periodicity) and 10×10^{-3} kyr^{-1}. These peaks show that the cyclicity is also present in the directly measured physical properties

spectral peak around 24×10^{-3} kyr^{-1} (41 kyr cl) is not evident. Thus, we do not observe an influence of the DWBC at Sites IV to VI, which implies that the DWBC does not reach that far into the Bounty Trough. We do observe frequencies of $(13–18) \times 10^{-3}$ kyr^{-1} (76–56 kyr cl) corresponding to shorter cycles than 100 kyrs at Sites IV and V. We attribute this observation to different periods between pairs of sea-level lowstands and age errors. For the last 800 kyr the general trend indicates an approximately 100 kyr cyclicity but the sea-level curve of Miller et al. (2005) is far from being regular. We infer that these peaks are caused by shorter periods (<100 kyrs) between some sea-level lowstands than 100 kyrs and the corresponding age uncertainties. We further conclude that Site IV documents a boundary and the DWBC does not cross to the west of this boundary.

Observing the influence on sediment deposition of the DWBC at Sites I to III and not at Sites IV to VI allows an estimation of the DWBC as a function of water depth. Analysing location and water depth of the different sites (Fig. 7), we can constrain the depth range of current activity to >3000 m (marked in Fig. 1b as white dashed line). Our findings confirm the presence of a deep cold limb of the DWBC (LCDW) inside the Bounty Trough, previously only inferred from observed erosion at the Outer Sill (Carter and McCave 1997). We thus conclude that the DWBC takes an active part in influencing the Bounty Trough sedimentary cover and has been present west of the Outer Sill even if today's core flow shifted southeast of Site I (Horn and Uenzelmann-Neben 2015) to a breach in the Bounty Channel levee (Carter et al. 1990). The upper depth limit of the DWBC conforms to the shallowest extent of the Lower Circumpolar Deep Water (LCDW Fig. 7) at about 2900 m (Carter et al. 2004b; McCave et al. 2008). We do not observe the influence of the DWBC via the 41 kyrs cl on sediments below Upper Circumpolar Deep Water (UCDW), which is also transported by the DWBC (McCave et al. 2008; Orsi et al. 1995) further west of Site III inside the Bounty Trough. UCDW has been identified in a maximum depth of 2500–2000 m west of New Zealand (Carter et al. 2004b; McCave et al. 2008). This indicates either a different water mass stratification inside the inner Bounty Trough compared to the flanks of the Campbell Plateau and Chatham Rise where the hydrological measurements (Profiles P14 and P15, see Fig. 1a; Talley 2007) were taken or a stronger link of the 41 kyrs cl to LCDW within the DWBC than to UCDW. One explanation could be the location of the Bounty Trough. The trough is more confined compared to the flanks of Campbell Plateau and the Chatham Rise. Additionally, another current may play a role. The Southland Current, (Figs. 1b, 7) flows from west to east through the area (McCave et al. 2008; Reid 1997). We suggest that the Southland Current may interact with

the UCDW via water mass mixing causing a different signature (assumed cyclicity every 100 kyrs, see "Oceanic setting of the Bounty Trough since the Pleistocene" section) inside the Bounty Trough or maybe even preventing UCDW from entering further into the Bounty Trough (see flow lines computed by Reid (1997) and arrows in Fig. 7). Thus, we can limit the influence of the DWBC to east of ~178.2°E. Further to the west the DWBC has not influenced sediment deposition during the late Quaternary. Sediments there mainly drape the underlying sedimentary bodies and no erosion has been reported west of 178.2°E (e.g. Carter et al. 1994; Uenzelmann-Neben et al. 2009).

The presence of the DWBC may have another effect. Recent research does not take into account the activity of the DWBC inside the middle Bounty Trough. It has been reported that in interglacial times (sea-level highstands) the Southland Current has a stronger northward than eastward limb and transports most of the terrigenous material derived from New Zealand past the head of Bounty Trough into the Hikurangi Channel further north (Carter and Carter 1993; Carter et al. 2004b). We thus conclude that during those warm periods the DWBC enters the Bounty Trough more strongly transporting cold LCDW and UCDW further west than during glacial times. UCDW and Southland Current may start mixing once the DWBC reaches the middle Bounty Trough thus changing water mass properties not only of UCDW but also of the water masses within the Southland Current. This in turn may affect the local surface water properties (Temperature, Salinity, nutrients?), prevent the Southland Current from extending further east towards the Outer Bounty Trough hence transporting warmth and vapours along the eastern New Zealand coast further to the north, and may have a feedback on local climate changing surface temperatures as well as primary productivity.

Using the method presented here a mapping of the regional extent of turbiditic versus current controlled sedimentation in relation to glacial/interglacial cycles is possible. Unfortunately, our dataset is not extensive enough for this. More high-resolution sediment echosounding seismic data lines across the Bounty Trough are need to achieve this task.

Conclusion

Spectral analysis of high resolution Parasound sub-bottom profiler data is capable of identifying the influence of the Pacific Deep Western Boundary Current (DWBC) within late Pleistocene sedimentary deposits of the Bounty Trough. This interpretation is supported by analysis of physical properties from ODP Site 1122.

We suggest a limb of the DWBC enters the Bounty Trough and is limited to east of 178.2°E (east of Site IV).
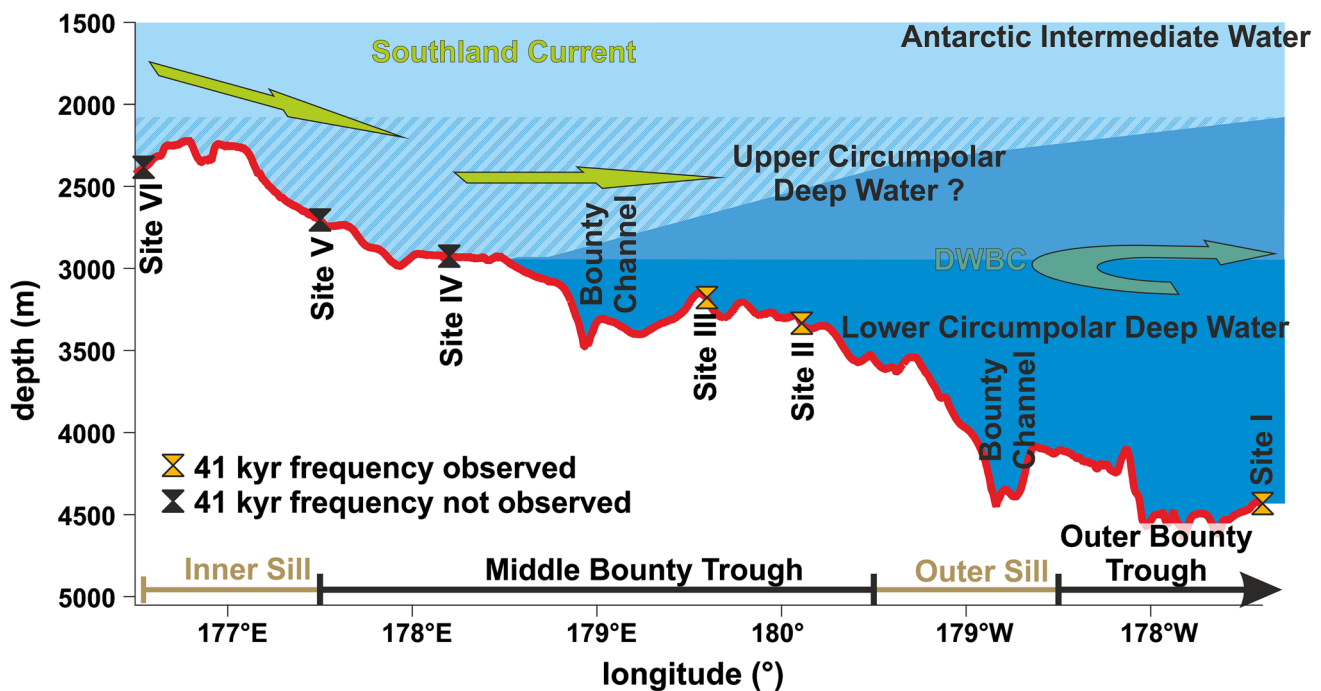
Fig. 7 Depth profile along the Bounty Trough. Site locations are indicated by *paired triangles*. The depth ranges water masses are marked in colour (Antarctic Intermediate Water in *light blue*, Circumpolar Deep Water in two *darker shades of blue*) in the Southwest Pacific Ocean, while *arrows* show the flow paths of currents (Southland Current, DWBC) (Carter et al. 2004b; McCave et al. 2008). We assume that Upper Circumpolar Deep Water interacts with the water masses in the Southland Current by mixing and/or displacement thus preventing it from entering the Bounty Trough

Previous studies could not establish the extent of the DWBC into the Bounty Trough; its existence was only inferred. With the knowledge of this extent we can assume that the DWBC was active inside the Bounty Trough during the last 100 kyrs, i.e. during the last glacial maximum and further into the past. This implies that cold waters were carried closer to New Zealand's South Island by the DWBC than presently assumed. Our findings may hence impact paleoclimate models for the New Zealand region. We infer that the western boundary of the DWBC follows the 3000 m depth isobath (Fig. 1b, white dashed line).

This method allows the chronological and regional distinction between more hemipelagic sedimentation as the result of a strong DWBC influence and downslope sedimentation due to sediment mass transport resulting from a strengthened eastward flowing Southland Current.

Key points

- Milankovitch cycles revealed in sub-bottom profiler data by spectral analysis.
- Inflow area of the DWBC illustrated by the 41 kyr Milankovitch cycle.

- Confirmation that DWBC is present in Bounty Trough area but only east of 178.15°E.

References

Atlas Hydrographic GmbH (2010) ATLAS PARASOUND Deep-Sea parametric sub-bottom profiler. http://www.atlas-elektronik.com/what-we-do/hydrographic-systems/parasound/, Bremen

Carter L, Carter RM (1988) Late quaternary development of left-bank-dominant levees in the Bounty Trough. N Z Mar Geol 78:185–197. doi:10.1016/0025-3227(88)90108-9

Carter L, Carter RM (1993) Sedimentary evolution of the Bounty Trough: a Cretaceous rift basin, southwestern Pacific Ocean. In: Ballance PF (ed) South Pacific Sedimentary Basins, vol 2., Sedimentary Basins of the WorldElsevier, Amsterdam, pp 51–67

Carter RM, Carter L (1996) The abyssal Bounty Fan and lower Bounty Channel: evolution of a rifted-margin sedimentary system. Mar Geol 130:181–202. doi:10.1016/0025-3227(95)00139-5

Carter L, McCave IN (1997) The sedimentary regime beneath the Deep Western Boundary Current inflow to the Southwest Pacific Ocean. J Sediment Res 67:1005–1017. doi:10.1306/d42686b2-2b26-11d7-8648000102c1865d

Carter L, Carter RM, Nelson CS, Fulthorpe CS, Neil HL (1990) Evolution of Pliocene to recent abyssal sediment waves on Bounty Channel levees. N Z Mar Geol 95:97–109. doi:10.1016/0025-3227(90)90043-J

Carter RM, Carter L, Davy B (1994) Seismic stratigraphy of the Bounty Trough, south-west Pacific Ocean. Mar Pet Geol 11:79–93. doi:10.1016/0264-8172(94)90011-6

Carter RM et al (1999) Site 1122: turbidites with a contourite foundation. In: Carter RM, McCave IN, Richter C, Carter L (eds) Proceedings of the ocean drilling program, initial reports, vol 181. Ocean Drilling Program, College Station. doi:10.2973/odp.proc.ir.181.106.2000

Carter L, Carter RM, McCave IN (2004a) Evolution of the sedimentary system beneath the deep Pacific inflow off eastern New Zealand. Mar Geol 205:9–27. doi:10.1016/s0025-3227(04)00016-7

Carter RM, McCave IN, Carter L (2004b) 1. Leg 181 synthesis: fronts, flows, drifts, vocanoes, and the evolution of the South-western Gateway to the Pacific Ocean, Eastern New Zealand. In: Richter C (ed) Proceedings of the ocean drilling programm, scientific results, vol 181. Ocean Drilling Program, College Station. doi:10.2973/odp.proc.sr.181.210.2004

Clark PU, Pisias NG, Stocker TF, Weaver AJ (2002) The role of the thermohaline circulation in abrupt climate change. Nature 415:863–869. doi:10.1038/415863a

Cooley JW, Tukey JW (1965) An algorithm for the machine calculation of complex. Fourier Ser Math Comput 19:297–301

Crundwell M, Scott G, Naish T, Carter L (2008) Glacial–interglacial ocean climate variability from planktonic foraminifera during the Mid-Pleistocene transition in the temperate Southwest Pacific, ODP Site 1123. Palaeogeogr Palaeoclimatol Palaeoecol 260:202–229. doi:10.1016/j.palaeo.2007.08.023

Davy B (1993) The Bounty Trough—basement structure influences on Sedimentary Basin evolution. In: Ballance PF (ed) South Pacific sedimentary basins. Sedimentary Basins of the World, vol 2. Elsevier, Amsterdam, pp 69–92

Erickson SN, Jarrard RD (1998) Velocity-porosity relationships for water-saturated siliciclastic sediments. J Geophys Res: Solid Earth 103:30385–30406. doi:10.1029/98jb02128

Gohl K (2003) Structure and dynamics of a submarine continent: tectonic-magmatic evolution of the Campbell Plateau (New Zealand) Report of the RV SONNE cruise SO-169, Project CAMP 17 January to 24 February 2003, vol 457. Alfred Wegner Institut, Helmholtz Centre for Polar and Marine Reseach, Bremerhaven. doi:10.2312/BzPM_0457_2003

Griggs GB, Carter L, Kennett JP, Carter RV (1983) Late Quaternary marine stratigraphy southeast of New Zealand. Geol Soc Am Bull 94:791–797. doi:10.1130/0016-7606(1983)94<791:lqmsso>2.0.co;2

Grobys JWG, Gohl K, Davy B, Uenzelmann-Neben G, Deen T, Barker D (2007) Is the Bounty Trough off eastern New Zealand an aborted rift? J Geophys Res: Solid Earth. doi:10.1029/2005JB004229

Hall IR, McCave IN, Shackleton NJ, Weedon GP, Harris SE (2001) Intensified deep Pacific inflow and ventilation in Pleistocene glacial times. Nature 412:809–812

Hall IR, McCave IN, Zahn R, Carter L, Knutz PC, Weedon GP (2003) Paleocurrent reconstruction of the deep Pacific inflow during the middle Miocene: reflections of East Antarctic ice sheet growth. Paleoceanography. doi:10.1029/2002pa000817

Hamilton EL (1978) Sound velocity–density relations in sea-floor sediments and rocks. J Acoust Soc Am 63:366–377. doi:10.1121/1.381747

Horn M, Uenzelmann-Neben G (2015) The Deep Western Boundary Current at the Bounty Trough, east of New Zealand: indications for its activity already before the opening of the Tasmanian Gateway. Mar Geol 362:60–75. doi:10.1016/j.margeo.2015.01.011

Kuhlbrodt T, Griesel A, Montoya M, Levermann A, Hofmann M, Rahmstorf S (2007) On the driving processes of the Atlantic meridional overturning circulation. Rev Geophys 45:RG2001. doi:10.1029/2004rg000166

Lu H, Fulthorpe CS, Mann P (2003) Three-dimensional architecture of shelf-building sediment drifts in the offshore Canterbury Basin. N Z Mar Geol 193:19–47. doi:10.1016/S0025-3227(02)00612-6

McCave IN, Carter L, Hall IR (2008) Glacial–interglacial changes in water mass structure and flow in the SW Pacific Ocean. Quatern Sci Rev 27:1886–1908. doi:10.1016/j.quascirev.2008.07.010

McCave IN, Crowhurst SJ, Kuhn G, Hillenbrand CD, Meredith MP (2014) Minimal change in Antarctic Circumpolar Current flow speed between the last glacial and Holocene. Nat Geosci 7:113–116. doi:10.1038/ngeo2037

Miller KG et al (2005) The phanerozoic record of global sea-level change. Science 310:1293–1298

Nafe JE, Drake CL (1957) Variation with depth in shallow and deep water marine sediments of porosity, density and the velocities of compressional and shear waves. Geophysics 22:523–552. doi:10.1190/1.1438386

Naish T et al (2009) Obliquity-paced Pliocene West Antarctic ice sheet oscillations. Nature 458:322–328. doi:10.1038/nature07867

Neil HL, Carter L, Morris MY (2004) Thermal isolation of Campbell Plateau, New Zealand, by the Antarctic circumpolar current over the past 130 kyr. Paleoceanography 19:PA4008. doi:10.1029/2003pa000975

Orsi AH, Whitworth T III, Nowlin WD Jr (1995) On the meridional extent and fronts of the Antarctic Circumpolar Current. Deep Sea Res Part I 42:641–673. doi:10.1016/0967-0637(95)00021-w

Osborn NI, Ciesielski PF, Ledbetter MT (1983) Disconformities and paleoceanography in the southeast Indian Ocean during the past 5.4 million years. Geol Soc Am Bull 94:1345–1358. doi:10.1130/0016-7606(1983)94<1345:dapits>2.0.co;2

Reid JL (1997) On the total geostrophic circulation of the pacific ocean: flow patterns, tracers, and transports. Prog Oceanogr 39:263–352. doi:10.1016/S0079-6611(97)00012-8

Schiel S (2009) The expedition of the research vessel" Polarstern" to the Antarctic in 2007 (ANT-XXIV/1) Berichte zur Polar-und Meeresforschung (Reports on polar and marine research), p 592

Sheriff RE, Geldart LP (1982) 4.3.2 Resolution. In: Exploration seismology Volume I: history, theory and data acquisition. Cambridge University Press, Cambridge, pp 117–122

Shipboard Scientific Party (2000) Site 1122: turbidites with a contourite foundation, vol 2. Ocean Drilling Program, College Station. doi:10.2973/odp.proc.ir.181.106.2000

Spiess V (1992) Digitale Sedimentechographie—Neue Wege zu einer hochauflösenden Akustostratigraphie, vol 35. Univerität Bremen, Bremen

Talley LD (2007) Pacific Ocean. The World Ocean Circulation Experiment (WOCE) hydrographic atlas series, vol 2. International WOCE Project Office, Southampton

Tiedemann R et al (2012) Cruise Report SO213: SOPATRA. Alfred Wegener Institute, Helmholtz Centre for Polar and Marine Research, Bremerhaven

Uenzelmann-Neben G, Grobys JWG, Gohl K, Barker D (2009) Neogene sediment structures in Bounty Trough, eastern New Zealand: influence of magmatic and oceanic current activity. Geol Soc Am Bull 121:134–149. doi:10.1130/B26259.1

Warren BA (1973) Transpacific hydrographic sections at Lats. 43°S and 28°S: the SCORPIO expedition—II. Deep Water Deep Sea Res Oceanogr Abst 20:9–38. doi:10.1016/0011-7471(73)90040-5

Weatherall P et al (2015) A new digital bathymetric model of the world's oceans. Earth Space Sci 2:331–345. doi:10.1002/2015ea000107

Weigelt E, Uenzelmann-Neben G (2007) Orbital forced cyclicity of reflector strength in the seismic records of the Cape Basin. Geophys Res Lett 34:L01702. doi:10.1029/2006gl028376

Zachos JC, Pagani M, Sloan L, Thomas E, Billups K (2001) Trends, rhythms, and aberrations in global climate 65 Ma to Present. Science 292:686–693